ISSN 0036-0236, Russian Journal of Inorganic Chemistry, 2023, Vol. 68, No. 9, pp. 1273–1281. © Pleiades Publishing, Ltd., 2023.
ISSN 0036-0236, Russian Journal of Inorganic Chemistry, 2023. © Pleiades Publishing, Ltd., 2023.
Russian Text © The Author(s), 2023, published in Zhurnal Neorganicheskoi Khimii, 2023, Vol. 68, No. 9, pp. 1303–1311.

COORDINATION COMPOUNDS

Controlling the Degree of Substitution of Lanthanides in Anionic Positions in Complexes $[CeNi_6(Ala)_{12}][(Ln_xCe_{1-x})(NO_3)_3(OH)_3(H_2O)]$

D. D. Semeshkina[a, *], Yu. A. Belousov[a, b], A. R. Savarets[a, c], M. V. Berekchiyan[a], and V. D. Dolzhenko[a, c]

[a] *Moscow State University, Moscow, 119991 Russia*
[b] *Lebedev Physical Institute, Russian Academy of Sciences, Moscow, 119991 Russia*
[c] *Zelinsky Institute of Organic Chemistry, Russian Academy of Sciences, Moscow, 119991 Russia*
**e-mail: semeshkina.d@gmail.com*

Received May 5, 2023; revised June 6, 2023; accepted June 6, 2023

Abstract—A series of 32 heterometallic ionic complexes $[CeNi_6(Ala)_{12}][(Ln_xCe_{1-x})(NO_3)_3(OH)_3(H_2O)]$ (Ln = Tb, Ho, Er, Tm, Yb, Lu) have been synthesized and characterized by XRD and IPC-MS. The dependence of the degree of substitution of lanthanides in the anionic position on the nature of Ln^{3+} and precipitation conditions has been determined. The processes occurring during the formation of the complexes have been studied by UV-Vis, diffuse reflectance electronic spectroscopy, and ICP-MS. Based on these data, a model of equilibria in the system was proposed to explain the increase in the degree of substitution of Ln in the anionic position in the lanthanide series and with a decrease in the concentration of Ce and Ln in the solution from which precipitation is performed.

Keywords: 3*d*–4*f* heterometallic complexes, lanthanides, nickel, amino acids, alanine degree of substitution
DOI: 10.1134/S0036023623601630

The unique physical properties of lanthanide ions are widely used in the design of luminescent and sensor materials [1–5], catalysts [6–10], lasers [11, 12], luminescent thermometers [13], and OLEDs [14–16]. Lanthanide coordination compounds are used in photodynamic therapy [17–19] and chemotherapy [20–22], as indicators for monitoring drug delivery [23–26], for immunoassay [27], and as contrast agents for magnetic resonance imaging [28, 29].

Some heterometallic complexes of lanthanides with 3*d* metals retain remanent magnetization for a certain time at low temperatures, which makes it possible to consider them potential single molecule magnets [30–36]. This causes not only fundamental, but also practical interest in 3*d*–4*f* lanthanide compounds.

Rational design of 3*d*–4*f* complexes requires ligands containing both "hard" and "soft" donor atoms exhibiting an affinity for "hard" 4*f* metals and "softer" 3*d* metals [37], which more often are copper, nickel, and cobalt. Natural amino acids satisfy this criterion [38–42].

A significant part of 3*d*–4*f* complexes with amino acids has the ratio Ln : M = 1 : 6, apparently due to the stability of the 3*d* cage [37]. The most common complexes are of two types (Fig. 1): trigonal prismatic, in which the 3*d*-metal atoms are located at the vertices of a trigonal prism around the central Ln atom, and octahedral, where the 3*d*-metal atoms are located at the vertices of an octahedron [37].

Trigonal prismatic complex cations do not have a pronounced preference for the ionic radius of the central lanthanide atom. For example, trigonal prismatic complexes with the $\{LnCo_6\}$ core have been obtained for almost the entire series Ln = La, Pr, Nd, Sm, Eu, Gd, Tb, Dy, Ho, Er, and Tm [43], which indicates an easy deformation of the cage. At the same time, octahedral-type complexes have a rigid cage and form only for lanthanides with the largest ionic radius [44, 45].

In such complexes with amino acids containing the $\{LnCu_6\}$ core, copper atoms are most often located at the vertices of a trigonal prism [46–49], while for $\{LnNi_6\}$ an octahedral structure is more typical [44, 45, 50, 51]. Only a small number of $\{LnCo_6\}$ complexes are known, among which there are structures of both octahedral [51, 52] and trigonal prismatic types [43].

Cobalt complexes are characterized by its oxidation during synthesis, as well as the formation of mixed-valence complexes [52]. This complicates the synthesis and hinders the study of processes in solution.

The selectivity of the formation of complex cations, resistance to oxidation, and other features of the structure and properties described above distinguish octa-

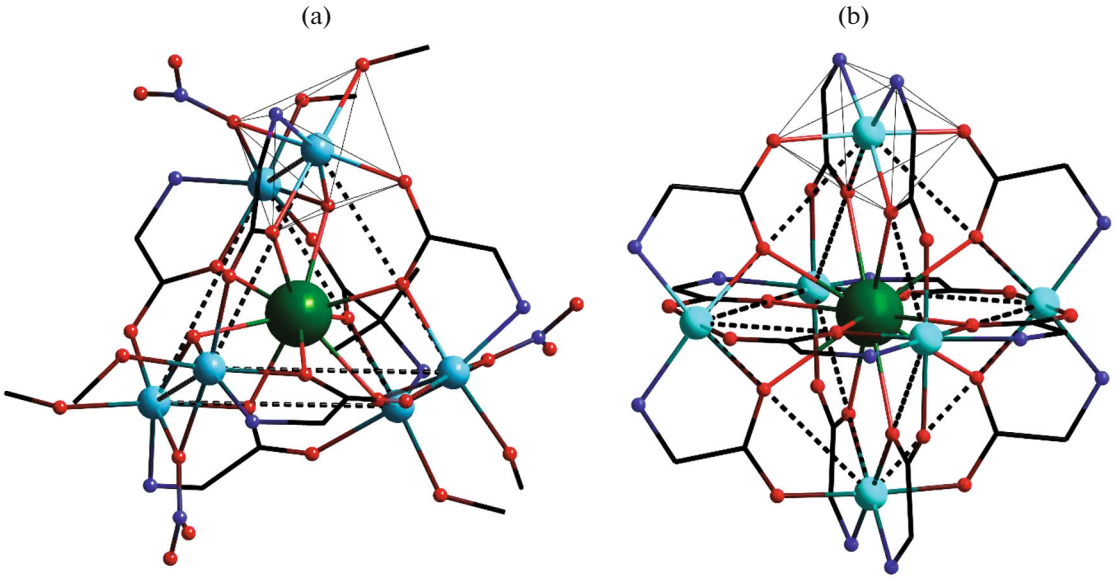

Fig. 1. $\{LnM_6\}$ complexes of (a) trigonal prismatic and (b) octahedral type.

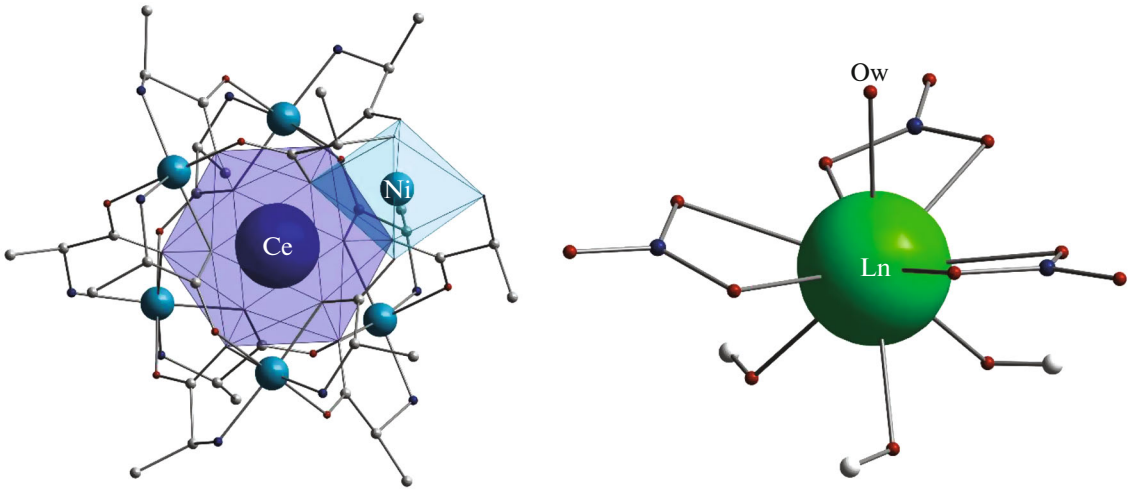

Fig. 2. Complex cation $[CeNi_6(Ala)_{12}]^{3+}$ and $[Ln(NO_3)_3(OH)_3(H_2O)]^{3-}$ counterion.

hedral *3d–4f* complexes of nickel with amino acids from other polynuclear heterometallic compounds.

As shown in [45], due to the presence of a rigid core, the cavity inside the $[LnNi_6(Ala)_{12}]^{3+}$ cation (Ala^- = L-alaninate ion) has a fixed size; as a result, such a complex is formed only for Ln = La–Nd, and as the lanthanide radius decreases, its stability decreases. The addition of an excess of lanthanide nitrate to a solution of the $[LnNi_6(Ala)_{12}]^{3+}$ complex gives $[LnNi_6(Ala)_{12}][(Ln(NO_3)_3(OH)_3(H_2O)]$ (Fig. 2). For complexes precipitated with gadolinium nitrate as an example, it has been shown that gadolinium in the anionic position in the resulting precipitate $[LnNi_6(Ala)_{12}][(Gd_xLn_{1-x})(NO_3)_3(OH)_3(H_2O)]$ can be partially replaced by the lighter lanthanide [45].

In this work, we studied the influence of the nature of the precipitating lanthanide on the degree of substitution of the Ln element in the anionic position of the $[CeNi_6(Ala)_{12}][(Ln_xCe_{1-x})(NO_3)_3(OH)_3(H_2O)]$ complexes (Ln = Tb, Ho, Er, Tm, Yb, Lu), as well as the possibility of controlling the degree of substitution.

EXPERIMENTAL

UV-Vis spectra were recorded on an SF-2000 spectrophotometer in quartz (1 cm) and glass (5 cm) cells. Diffuse reflectance electronic spectra (DRS) were

recorded on a Shimadzu UV-2600i spectrophotometer with the use of an IRS-2600Plus integrating sphere. X-ray diffraction analysis was performed on a Rigaku D/MAX 2500 diffractometer in the reflection mode with a copper anode ($CuK_{\alpha 1}$) and a graphite monochromator in the 2θ angle range 5°–60°. X-ray powder diffraction patterns were analyzed using the STOE WinXPOW software. The IR spectra of compounds were recorded on a Perkin-Elmer Spectrum 65 FTIR spectrophotometer in the range 4000–400 cm^{-1}. Inductively coupled plasma mass spectra (ICP-MS) were recorded on a Perkin-Elmer ELAN DRC-II mass spectrometer.

Lanthanide nitrate solutions were standardized by complexometric titration at pH 5.4 with photometric fixation of the end point of the titration; Xylenol Orange was used as an indicator.

Synthesis of $[Ni(Ala)_2(H_2O)_2]\cdot 2H_2O$. From an aqueous solution of 5.89 g (0.0548 mol) of $Ni(NO_3)_2\cdot 6H_2O$, an amorphous $Ni(OH)_2$ was precipitated by adding a NaOH solution, washed with water by decantation until the sedimentation of the precipitate stopped, filtered, and then 9.8 g (0.11 mol) of L-alanine and 600 mL of water were added. The solution was heated with stirring until complete dissolution of the hydroxide. The hot blue solution was filtered and evaporated until crystallization began. After cooling, the precipitate was filtered off and recrystallized from a minimum amount of water. The precipitated crystals were filtered off, washed with ice water and alcohol, and dried in a vacuum. The crystals had an intense blue color immediately after preparation, but upon storage it became pale. The yield was 10.5 g (70.5%). X-ray powder diffraction data correspond to the literature data [53]. DRS spectrum was recorded for the solid substance (Fig. 3a). For a solution in methanol ($C = 0.038$ mol/L), the UV-Vis spectra were recorded (Fig. 3b), which were decomposed by the least-squares method into Gaussians corresponding to electronic transitions [54], the background was described using Thompson and Rayleigh scattering. From the data obtained, the splitting parameters in the crystal field were estimated: $\Delta_O = 9260$ cm^{-1} for solid $Ni(Ala)_2$ and $\Delta_O < 9000$ cm^{-1} for a methanol solution. The change in Δ_O most likely indicates a change in the nearest coordination environment of nickel due to the replacement of H_2O molecules by MeOH. Due to the low solubility in ethanol, it was not possible to record an UV-Vis spectrum for it.

Synthesis of the $[CeNi_6(Ala)_{12}]^{3+}$ cation in solution. A 10% excess of solid nickel alaninate was added to a standardized ethanol solution of $Ce(NO_3)_3$ ($C = 0.0275$ mol/L, $V = 100$ mL). The resulting suspension was stirred with heating for 15 min until the solution turned purple. Initially, on heating, along with unreacted $Ni(Ala)_2$, a violet precipitate of $[CeNi_6(Ala)_{12}][Ce(NO_3)_3(OH)_3(H_2O)]$ was formed, which completely dissolved upon further heating. The color of the remaining precipitate corresponded to the excess nickel alaninate, which was then filtered off.

$$Ce(NO_3)_3 + 6Ni(Ala)_2 = [CeNi_6(Ala)_{12}](NO_3)_{3(sol)}.$$

The filtrate was transferred to a 100-mL volumetric flask and made up to the mark. The concentration of the complex cation was assumed to be equal to the initial concentration of cerium, because, according to ICP-MS data, the solution obtained in this way contains Ce and Ni in a ratio of 1 : 6, which confirms the complete transition of cerium to the $[CeNi_6(Ala)_{12}]^{3+}$ form. For Ce, when nitrate is used as the initial reagent, the resulting solutions are highly stable during storage.

Synthesis of compounds of the composition $[CeNi_6(Ala)_{12}][(Ln_xCe_{1-x})(NO_3)_3(OH)_3(H_2O)]$ (Ln = Tb, Ho, Er, Tm, Yb, Lu). All precipitates were obtained by the same procedure, varying only the total volume of the solution (V_{tot}) and the nature of lanthanide nitrate used as a precipitant. To 1 mL of a solution of the complex cation $[CeNi_6(Ala)_{12}]^{3+}$ (1 equiv), ($V_{tot} - 2$) mL of ethanol and then 1 mL of a solution of the precipitant ($Ln(NO_3)_3$, 2 equiv) were added. The precipitated finely crystalline powders were filtered off and dried in air.

Determination of the Ln/Ce molar ratio in $[CeNi_6(Ala)_{12}][(Ln_xCe_{1-x})(NO_3)_3(OH)_3(H_2O)]$ by ICP-MS. Analyte samples weighing ~3 mg were placed in 25-mL volumetric flasks, then 1 mL of HNO_3(conc) was added to destroy the complex, and 50 μL of a standard solution of rhodium chloride ($C_{Rh} = 0.002$ mol/L) was added as an internal reference, and the solution was made up to the mark with deionized water. Standard solutions were prepared by diluting Inorganic Ventures multi-element standard Ln CCS-1 with a concentration of 100 mg/L and a nickel standard solution with a Ni content of 1000 mg/L to obtain solutions with lanthanide concentrations in the range of 0.003–0.066 μmol/mL and Ni 0.02–0.4 μmol/mL. To each solution, 1 mL HNO_3(conc.) and an aliquot of a standard rhodium chloride solution were added. The analytical signal was measured on ^{103}Rh, ^{58}Ni, ^{140}Ce, ^{159}Tb, ^{165}Ho, ^{166}Er, ^{169}Tm, ^{173}Yb, and ^{175}Lu nuclei.

UV-Vis spectra of solutions over the precipitates. After the crystallization of the powders $[CeNi_6(Ala)_{12}][(Ln_xCe_{1-x})(NO_3)_3(OH)_3(H_2O)]$ (Ln = Tb, Yb, Lu; $V_{tot} = 7$ mL) was completed, the solutions above the precipitates were filtered, then UV-Vis spectra were recorded in the wavelength range 400–700 nm ($l = 1$ cm).

A decrease in the concentration of $[CeNi_6(Ala)_{12}]^{3+}$ was observed in the presence of Lu^{3+}. A solution of $Lu(NO_3)_3$ (2 equiv) was added to the

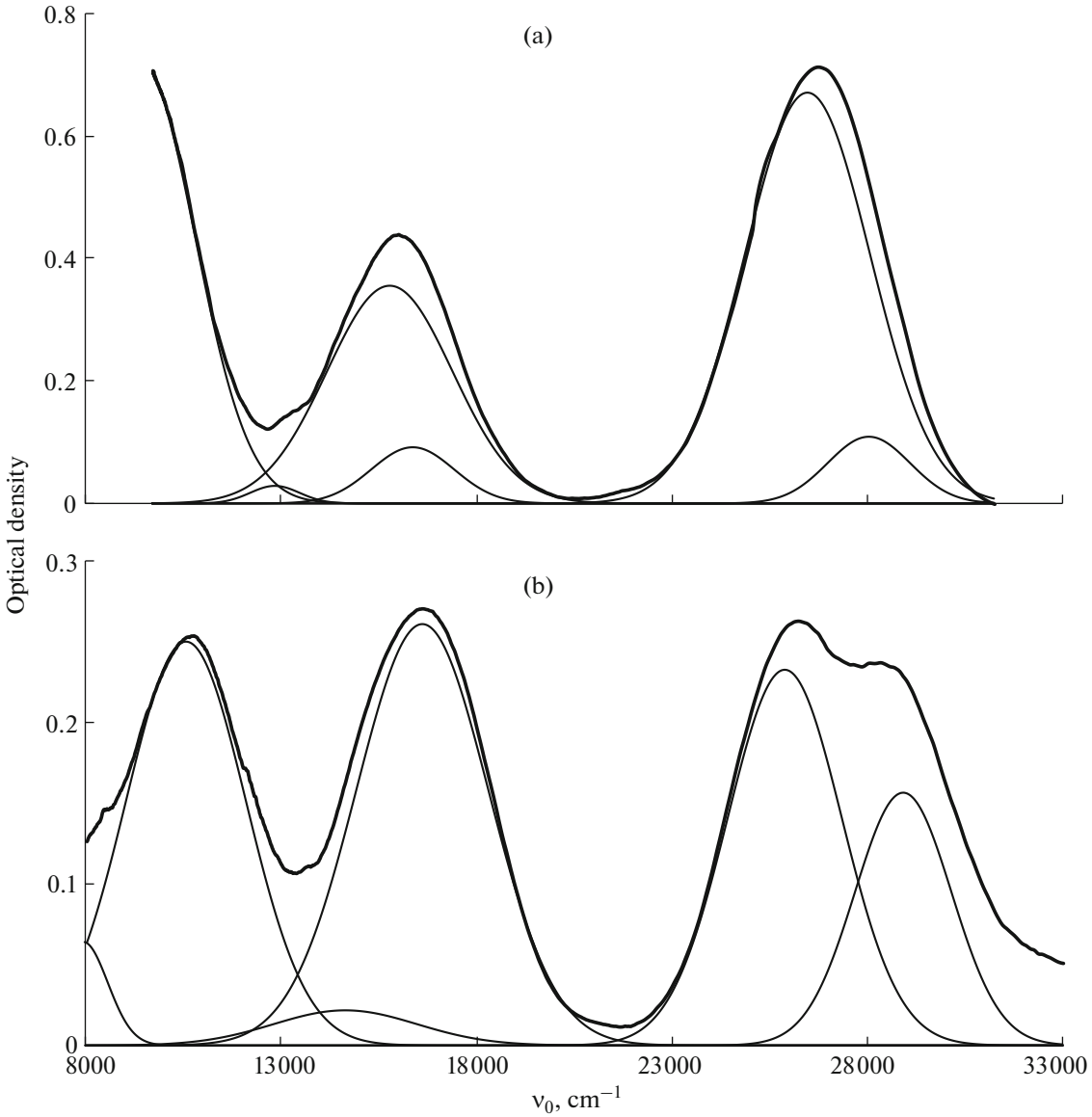

Fig. 3. (a) DRS spectra of $Ni(Ala)_2$ and (b) UV-Vis spectra of a solution of $Ni(Ala)_2$ in methanol.

$[CeNi_6(Ala)_{12}]^{3+}$ solution (in the resulting solution $C_{Ce} = 0.0013$ mol/L, $C_{Lu} = 0.0026$ mol/L) and a series of UV-Vis spectra were recorded in cells with $l = 5$ cm in wavelength range 400–1000 nm. The change in the concentration of the heterometallic cation with time was determined.

RESULTS AND DISCUSSION

A series of samples with the $[CeNi_6(Ala)_{12}]^{3+}$ cation was synthesized. The cation was precipitated with two equivalents of nitrates Ln = Tb, Ho, Er, Tm, Yb, and Lu varying the concentration of lanthanides in the solution. The samples obtained were characterized by X-ray powder diffraction, IR spectroscopy, and ICP-MS. According to XRD data, all obtained samples are isostructural (Fig. 4). The IR spectra of all samples are similar (Fig. 5) and correspond to the previously described complexes $[CeNi_6(Ala)_{12}][Gd(NO_3)_3(OH)_3(H_2O)]$ [45].

According to XRD data, the crystal structure contains $[CeNi_6(Ala)_{12}]^{3+}$ complex cations of the octahedral type, in which the Ce^{3+} ion is located in the cage formed by $Ni(Ala)_2$ fragments (Fig. 2) [45]. In the solution formed upon the interaction of an ethanol solution of cerium nitrate with an excess of nickel alaninate, the Ce/Ni concentration ratio, according to ICP-MS data, is 1 : 6. The maxima in the UV-Vis spectrum of this solution coincide with the maxima in the DRS spectra of $[CeNi_6(Ala)_{12}][(Lu_{0.5}Ce_{0.5})(NO_3)_3(OH)_3(H_2O)]$ powders (Fig. 6), which is evidence that cerium and

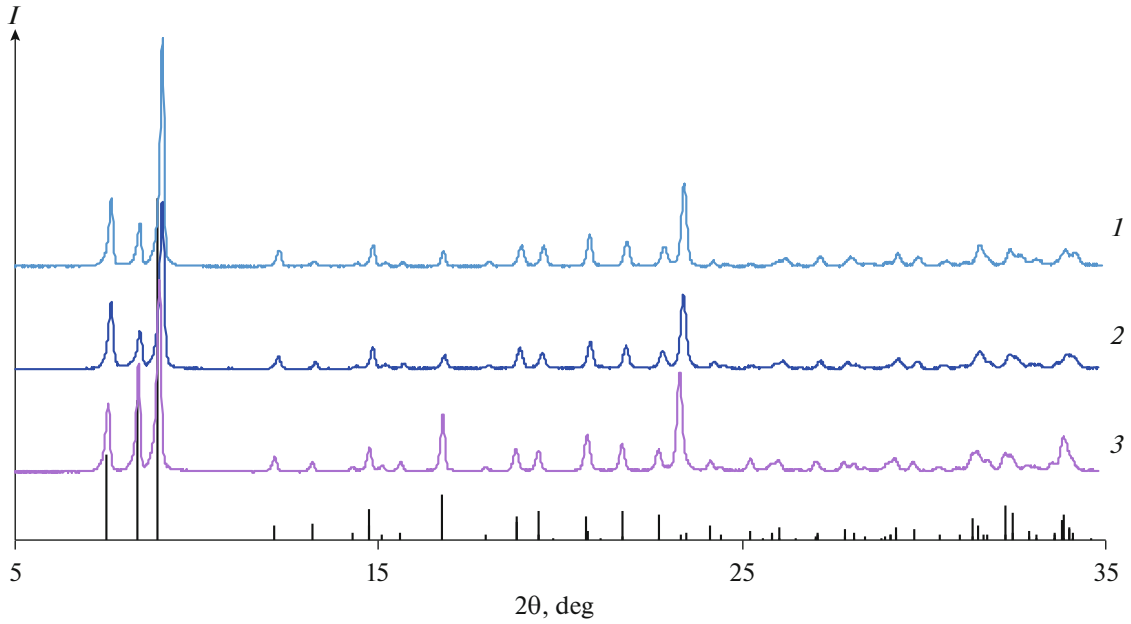

Fig. 4. X-ray powder diffraction patterns of the $[CeNi_6(Ala)_{12}][(Ho_xCe_{1-x})(NO_3)_3(OH)_3(H_2O)]$ complexes obtained from solutions with V_{tot} = (*1*) 2, (*2*) 3, and (*3*) 4 mL.

nickel ions in solution are present only in the heterometallic cation $[CeNi_6(Ala)_{12}]^{3+}$, which precipitates unchanged. The UV-Vis spectrum of the $[CeNi_6(Ala)_{12}]^{3+}$ solution and the DRS spectrum of $[CeNi_6(Ala)_{12}][(Lu_xCe_{1-x})(NO_3)_3(OH)_3(H_2O)]$were decomposed into Gaussian components using the least-squares method and the position of the absorption maxima was determined (Table 1); the assignment of absorption bands was carried out in accordance with [54].

In the crystal structure of the complex (Fig. 7), cerium atoms are distributed over cationic ($[CeNi_6(Ala)_{12}]^{3+}$) and anionic ($[Ce(NO_3)_3(OH)_3(H_2O)]^{3-}$) positions. We have estimated the Ln/Ce molar ratio in the precipitate, which is related to the degree of substitution $(1 - x)$. For $[CeNi_6(Ala)_{12}][Ln(NO_3)_3(OH)_3(H_2O)]$, the ratio is Ln/Ce = 1. Upon substitution of Ln^{3+} in the anionic position, the precipitate has the composition $[CeNi_6(Ala)_{12}][(Ln_xCe_{1-x})(NO_3)_3(OH)_3(H_2O)]$ and Ln/Ce < 1. The higher the degree of substitution, the lower the Ln/Ce ratio.

It is difficult to directly determine the equilibrium concentrations of the $[CeNi_6(Ala)_{12}]^{3+}$ cation and the $[Ln(NO_3)_3(OH)_3(H_2O)]^{3-}$ anion; therefore, instead of the product of the concentrations of the cation and anion, we used $-\log(C_{Ce}\cdot C_{Ln})$ (Fig. 8). On the graph, the concentrations of the initial solutions decrease from left to right.

The substitution of Ln^{3+} in the anionic position depends on the nature of the lanthanide and precipitation conditions. In the series of lanthanides for crystals obtained under the same conditions, the fraction of Ce in the anionic position increases. Upon dilution of the initial solution, the substitution of Ln^{3+} in the anionic position by Ce^{3+} increases for all lanthanides. To explain the observed regularities, this system was studied in detail and a model of the processes occurring in it was proposed.

(1) Within the framework of the model approximation, the nature of the lanthanide has practically no effect on the solubility product of the complex precip-

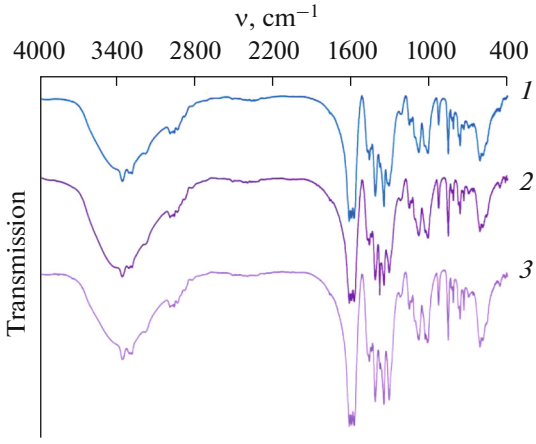

Fig. 5. IR spectra of the $[CeNi_6(Ala)_{12}][(Yb_xCe_{1-x})(NO_3)_3(OH)_3(H_2O)]$ complexes obtained from solutions with V_{tot} = (*1*) 2.5, (*2*) 3.5, and (*3*) 7 mL.

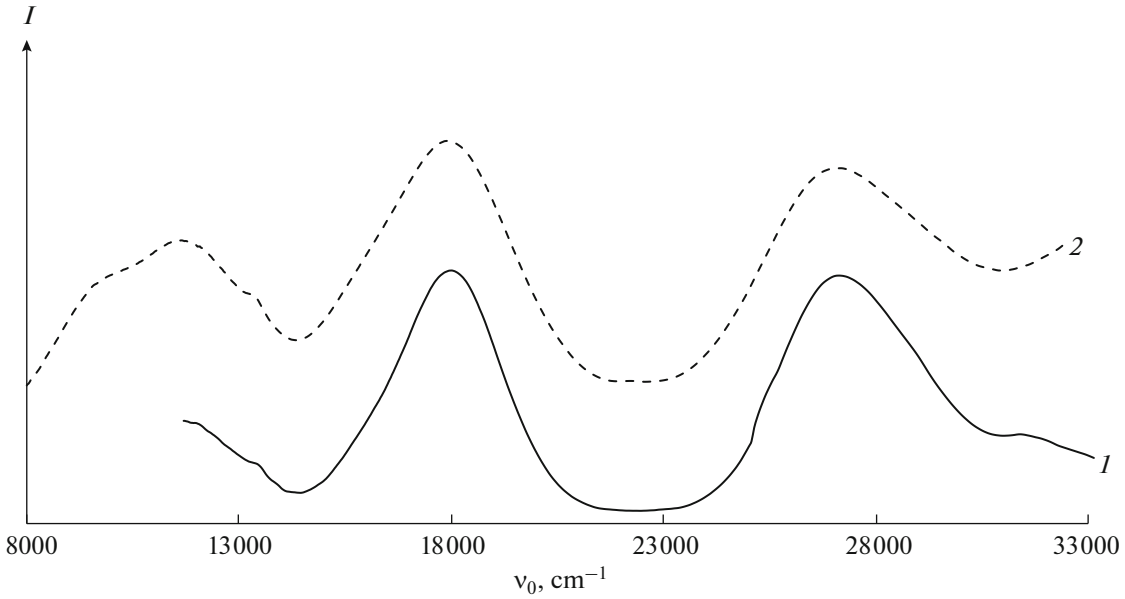

Fig. 6. (*1*) UV-Vis spectrum of a solution of $[CeNi_6(Ala)_{12}]^{3+}$ and (*2*) DRS spectrum of $[CeNi_6(Ala)_{12}][(Lu_{0.5}Ce_{0.5})(NO_3)_3(OH)_3(H_2O)]$.

itate, since all precipitates are isostructural (according to X-ray powder diffraction data), and the cation and anion radii are close. Equilibrium

$$[CeNi_6(Ala)_{12}]^{3+} + [Ln'(NO_3)_3(OH)_3(H_2O)]^{3-} \rightleftarrows [CeNi_6(Ala)_{12}][Ln'(NO_3)_3(OH)_3(H_2O)]\downarrow$$
$$(Ln' = Ce, Tb-Lu)$$

is characterized by the constant $K_{SP} = [K]([A_{Ce}] + [A_{Ln}])$, where $K = [CeNi_6(Ala)_{12}]^{3+}$, $A_{Ln} = [Ln(NO_3)_3(OH)_3(H_2O)]^{3-}$, and $A_{Ce} = [Ce(NO_3)_3(OH)_3(H_2O)]^{3-}$.

(2) The equilibrium concentration of the complex cation [K] in solutions above the precipitate after reaching equilibrium (the end of crystallization) monotonically increases in the lanthanide series (Fig. 9); therefore, the total equilibrium concentration of anions ($[A_{Ce}] + [A_{Ln}]$) monotonically decreases. This results in a decrease in $[A_{Ln}]$ in the lanthanide series and, as a consequence, a decrease in the stability of the anionic complex $[Ln(NO_3)_3(OH)_3(H_2O)]^{3-}$.

(3) Figure 10 shows the change in the $[CeNi_6(Ala)_{12}]^{3+}$ concentration over time in the presence of Lu^{3+}. It can be seen that the heterometallic cation is destroyed:

$$[CeNi_6(Ala)_{12}]^{3+} \xrightarrow{Ln^{3+}} Ce^{3+}.$$

The released cerium is able to form the anionic complex $[Ce(NO_3)_3(OH)_3(H_2O)]^{3-}$, which can also be a part of the crystalline precipitate $[CeNi_6(Ala)_{12}][Ln'(NO_3)_3(OH)_3(H_2O)]$ (Ln' = Ce, Tb–Lu).

(4) $[A_{Ln}]$ decreases in going from Tb^{3+} to Lu^{3+}, which requires a higher $[A_{Ce}]$ concentration to reach $K_{SP} = [K]([A_{Ce}] + [A_{Ln}])$. The content of Ce in the anionic position increases, and the degree of substitution increases in the lanthanide series.

(5) When the solution is diluted, [K] and $[A_{Ln}]$ decrease, which requires a more significant increase in $[A_{Ce}]$ to achieve K_{SP} compared to the undiluted solution; this explains the increase in the degree of substitution when the initial solution is diluted.

CONCLUSIONS

Samples of the composition $[CeNi_6(Ala)_{12}][(Ln_xCe_{1-x})(NO_3)_3(OH)_3(H_2O)]$ (Ln = Tb, Ho, Er, Tm, Yb, Lu) have been synthesized from solutions with various C_{Ce} and C_{Ln} values and studied by XRD, ICP-MS, and IR spectroscopy. It has been shown that the degree of substitution of lanthanides in the anionic position increases both with a decrease in C_{Ce} and C_{Ln} in the initial solution and with

Table 1. Electronic transitions in the $[CeNi_6(Ala)_{12}]^{3+}$ complex

Excited state term	$^3T_{1g}(B_1)$	$^3T_{1g}(A_2)$	$^3T_{1g}(A_2)$	$^3T_{1g}(B_1)$	$^1E_g(^1B_1, {}^1A_1)$	$^3T_{2g}(A_2)$	$^3T_{2g}(A_1)$
ν_0, cm^{-1}	28320	26380	17910	15540	13460	11670	9350

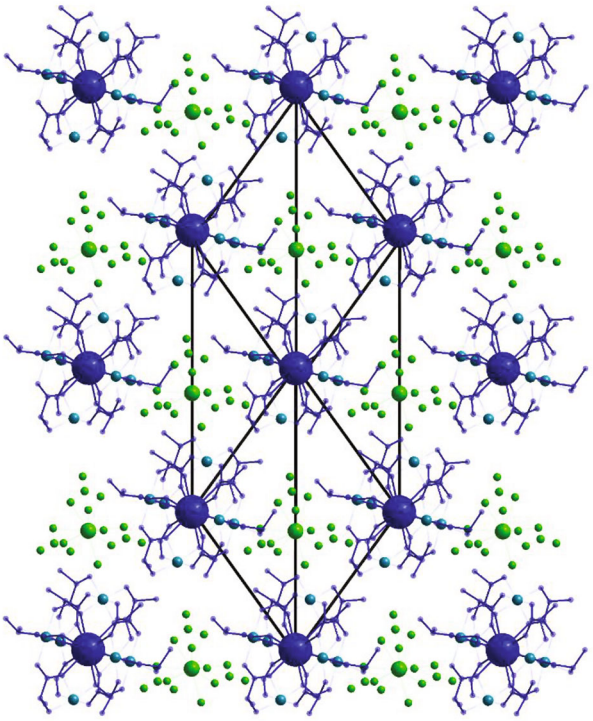

Fig. 7. Crystal structure of $[CeNi_6(Ala)_{12}][(Ln_xCe_{1-x})(NO_3)_3(OH)_3(H_2O)]$ [45].

a decrease in the ionic radius of Ln^{3+}. A model of processes in this system has been proposed and confirmed by a combination of physicochemical methods, which explains the observed regularities.

According to the proposed model, in the solution of the $[CeNi_6(Ala)_{12}]^{3+}$ cation in the presence of Ln^{3+}, destruction processes occur, and the cerium released in this case forms the $[Ce(NO_3)_3(OH)_3(H_2O)]^{3-}$ complex anion. The stability and equilibrium concentration of the $[Ln(NO_3)_3(OH)_3(H_2O)]^{3-}$ anions decrease in the lanthanide series, and the fraction of cerium in the precipitate increases in going from Tb to Lu. When the initial solution is diluted, the equilibrium concentrations of $[CeNi_6(Ala)_{12}]^{3+}$ and $[Ln(NO_3)_3(OH)_3(H_2O)]^{3-}$ decrease, so the degree of substitution of cerium for Ln in the anionic position increases. At high concentrations of Ce and Ln, a precipitate of the composition $[CeNi_6(Ala)_{12}][Ln(NO_3)_3(OH)_3(H_2O)]$ (Ln : Ce = 1 : 1) is formed; at low concentrations, the $[CeNi_6(Ala)_{12}][Ce(NO_3)_3(OH)_3(H_2O)]$ precipitate (Ln : Ce = 0 : 1) is formed. Thus, the dependence of Ln/Ce on $\ln(C_{Ce}\ C_{Ln})$ should be described by a decreasing S-shaped curve.

The shape and position of this curve are determined by the nature of Ln. Apparently, in the studied range of concentrations in Fig. 8, we observe different

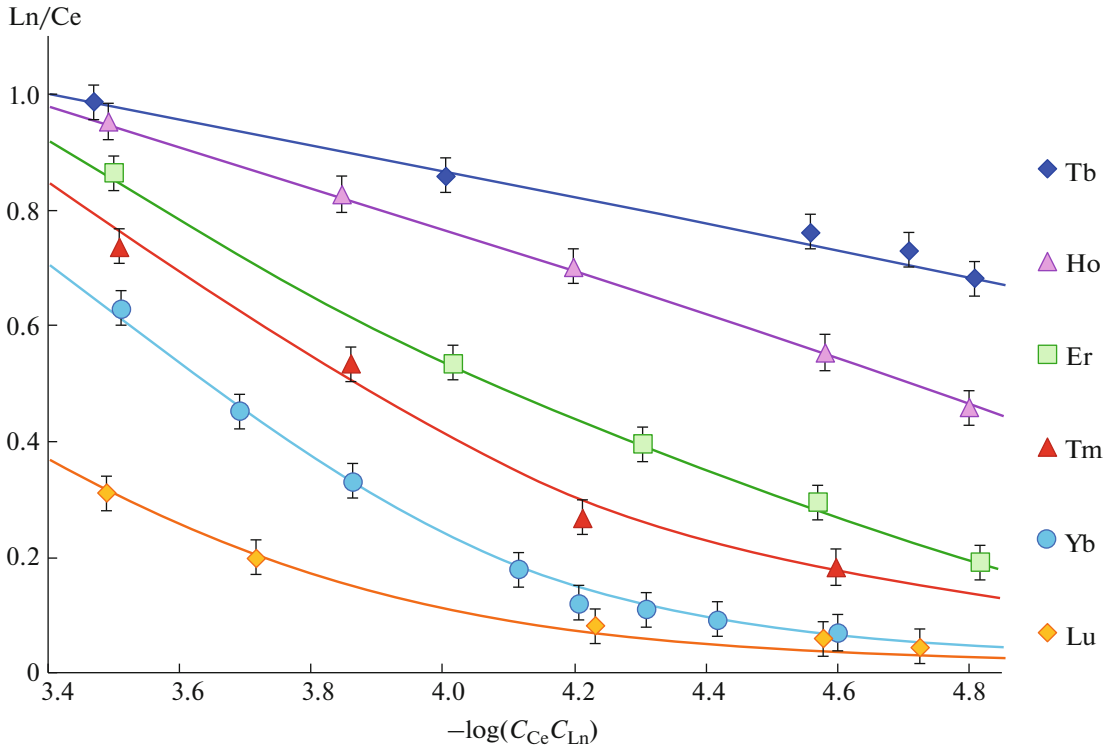

Fig. 8. Dependence of the degree of substitution of Ln^{3+} in the anionic position on the nature of lanthanide and precipitation conditions.

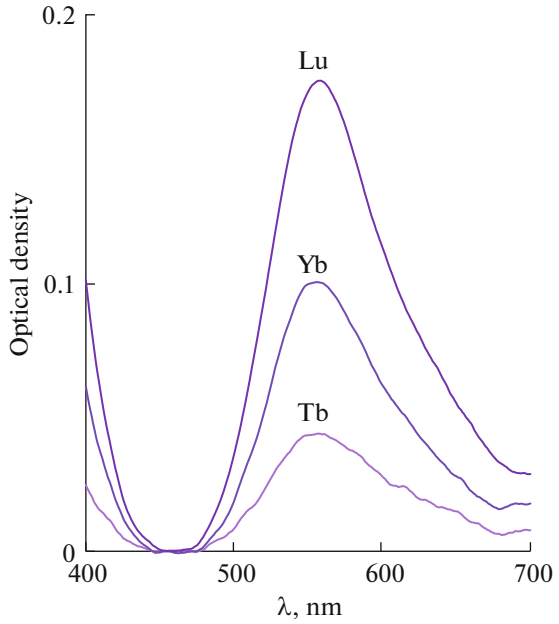

Fig. 9. UV-Vis of solutions over precipitates after the end of crystallization obtained from solutions with $V_{tot} = 7$ mL.

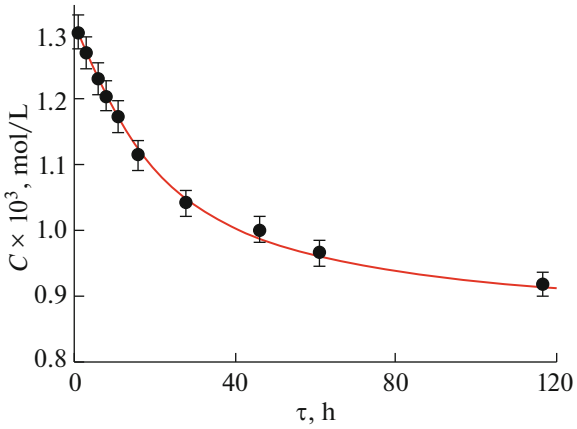

Fig. 10. Change in concentration of $[CeNi_6(Ala)_{12}]^{3+}$ over time in the presence of Lu^{3+}.

segments of the S-shaped curve: initial for Tb and Ho (Ln/Ce ~ 1 at the first point), intermediate for Er and Tm (significant change in Ln/Ce, 0.9–0.2), final for Yb and Lu (asymptotic tendency to zero on the right side of the graph).

Thus, the composition of $[CeNi_6(Ala)_{12}][(Ln_xCe_{1-x})(NO_3)_3(OH)_3(H_2O)]$ precipitates can be controlled by varying the concentration of Ce and Ln in the solution from which the precipitation is made, at a fixed molar ratio of Ce and Ln ions. To increase the proportion of cerium in the precipitate, it is necessary to reduce supersaturation, and to increase the Ln content, it is necessary to carry out precipitation from more concentrated solutions.

CONFLICT OF INTEREST

The authors declare no conflicts of interest.

REFERENCES

1. V. E. Gontcharenko, A. M. Lunev, I. V. Taydakov, et al., IEEE Sens. J. **19**, 7365 (2019). https://doi.org/10.1109/JSEN.2019.2916498
2. A. M. Lunev and Y. A. Belousov, Russ. Chem. Bull. **71**, 825 (2022). https://doi.org/10.1007/S11172-022-3485-3
3. D. A. Kordeyro Magrino, V. M. Korshunov, K. A. Lyssenko, et al., Inorg. Chim. Acta **510**, 119764 (2020). https://doi.org/10.1016/J.ICA.2020.119764
4. I. V. Taydakov, V. M. Korshunov, Y. A. Belousov, et al., Inorg. Chim. Acta **513**, 119922 (2020). https://doi.org/10.1016/J.ICA.2020.119922
5. C. Pettinari, F. Marchetti, R. Pettinari, et al., Dalton Trans. **44**, 14887 (2015). https://doi.org/10.1039/C5DT01964H
6. Z. H. Pan, Z. Z. Weng, X. J. Kong, et al., Coord. Chem. Rev. **457**, 214419 (2022). https://doi.org/10.1016/j.ccr.2022.214419
7. A. C. Ferreira, J. F. Martinho, and J. B. Branco, ChemCatChem **14**, 1 (2022). https://doi.org/10.1002/cctc.202101548
8. D. J. Bell, L. S. Natrajan, and I. A. Riddell, Coord. Chem. Rev. **472**, 214786 (2022). https://doi.org/10.1016/j.ccr.2022.214786
9. C. Zhu, Y. Zhou, J. Yang, et al., Org. Chem. Front. **10**, 1263 (2023). https://doi.org/10.1039/d2qo01930b
10. E. C. Moinet, B. M. Wolf, O. Tardif, et al., Angew. Chem., Int. Ed. Engl. **62** (2023). https://doi.org/10.1002/anie.202219316
11. Y. Xie, Y. Song, G. Sun, et al., Light Sci. Appl. **11**, 813 (2022). https://doi.org/10.1038/s41377-022-00813-9
12. F. Jobin, P. Paradis, Y. O. Aydin, et al., Opt. Express **30**, 8615 (2022). https://doi.org/10.1364/oe.450929
13. Y. A. Belousov, A. A. Drozdov, I. V. Taydakov, et al., Coord. Chem. Rev. **445**, 214084 (2021). https://doi.org/10.1016/J.CCR.2021.214084
14. A. Barkanov, A. Zakharova, T. Vlasova, et al., J. Mater. Sci. **57**, 8393 (2022). https://doi.org/10.1007/s10853-021-06721-4
15. R. Ilmi, D. Zhang, L. Tensi, et al., Dyes Pigm. **203**, 300 (2022). https://doi.org/10.1016/j.dyepig.2022.110300
16. D. A. Metlina, D. O. Goryachii, M. T. Metlin, et al., Materials **16**, 31243 (2023). https://doi.org/10.3390/ma16031243
17. M. Galland, T. Le Bahers, A. Banyasz, et al., Chem.—A Eur. J. **25**, 9026 (2019). https://doi.org/10.1002/chem.201901047
18. S. Dasari, S. Singh, S. Sivakumar, et al., Chem.—A Eur. J. **22**, 17387 (2016). https://doi.org/10.1002/chem.201603453

19. C. Xie, H. F. Chau, J. X. Zhang, et al., Adv. Ther. **2**, 1900068 (2019). https://doi.org/10.1002/adtp.201900068

20. M. P. al Campello, E. Palma, I. Correia, et al., Dalton Trans. **48**, 4611 (2019). https://doi.org/10.1039/c9dt00640k

21. Y. C. Liu, Z. F. Chen, X. Y. Song, et al., Eur. J. Med. Chem. **59**, 168 (2013). https://doi.org/10.1016/j.ejmech.2012.11.001

22. W. L. Kwong, R. Wai-Yin Sun, C. N. Lok, et al., Chem. Sci. **4**, 747 (2013). https://doi.org/10.1039/c2sc21541a

23. H. Li, C. Xie, R. Lan, et al., J. Med. Chem. **60**, 8923 (2017). https://doi.org/10.1021/acs.jmedchem.7b01162

24. H. Li, R. Lan, C. F. Chan, et al., Chem. Commun. **51**, 14022 (2015). https://doi.org/10.1039/c5cc05461c

25. H. Li, B. I. Harriss, A. Phinikaridou, et al., Nanotheranostics **1**, 186 (2017). https://doi.org/10.7150/ntno.18619

26. A. Chandra, K. Singh, S. Singh, et al., Dalton Trans. **45**, 494 (2016). https://doi.org/10.1039/c5dt04470g

27. E. G. Moore, A. P. S. Samuel, and K. N. Raymond, Acc. Chem. Res. **42**, 542 (2009). https://doi.org/10.1021/ar800211j

28. E. Kanal, Magn. Reson. Imaging **34**, 1341 (2016). https://doi.org/10.1016/j.mri.2016.08.017

29. M. F. Bellin and A. J. Van Der Molen, Eur. J. Radiol. **66**, 160 (2008). https://doi.org/10.1016/j.ejrad.2008.01.023

30. C. A. P. Goodwin, F. Ortu, D. Reta, et al., Nature **548** (7668), 439 (2017). https://doi.org/10.1038/nature23447

31. F. S. Guo, B. M. Day, Y. C. Chen, et al., Angew. Chem., Int. Ed. Engl. **56**, 11445 (2017). https://doi.org/10.1002/anie.201705426

32. PiquerL. Rosado and E. C. Sanudo, Dalton Trans. **44**, 8771 (2015). https://doi.org/10.1039/c5dt00549c

33. J. T. Chen, H. Yan, T. T. Wang, et al., Inorg. Chem. **61**, 19097 (2022). https://doi.org/10.1021/acs.inorgchem.2c02474

34. M. Georgiev and H. Chamati, ACS Omega **7**, 42664 (2022). https://doi.org/10.1021/acsomega.2c06119

35. C. M. Liu, R. Sun, B. W. Wang, et al., Inorg. Chem. **61**, 18510 (2022). https://doi.org/10.1021/acs.inorgchem.2c02743

36. F. A. Mautner, F. Bierbaumer, R. C. Fischer, et al., Inorg. Chem. **61**, 11124 (2022). https://doi.org/10.1021/acs.inorgchem.2c00958

37. A. B. Canaj, F. Kakaroni, A. Collet, et al., Polyhedron **151**, 1 (2018). https://doi.org/10.1016/j.poly.2018.05.005

38. N. Stavgianoudaki, M. Siczek, T. Lis, et al., Chem. Commun. **52**, 343 (2016). https://doi.org/10.1039/c5cc07243c

39. T. Peristeraki, M. Samios, M. Siczek, et al., Inorg. Chem. **50**, 5175 (2011). https://doi.org/10.1021/ic2004744

40. A. Hosoi, Y. Yukawa, S. Igarashi, et al., Chem.—A Eur. J. **17**, 8264 (2011). https://doi.org/10.1002/chem.201100769

41. Y. Yukawa, G. Aromi, S. Igarashi, et al., Angew. Chem., Int. Ed. Engl. **44**, 1997 (2005). https://doi.org/10.1002/anie.200462401

42. X. J. Kong, Y. P. Ren, L. S. Long, et al., J. Am. Chem. Soc. **129**, 7016 (2007). https://doi.org/10.1021/ja0726198

43. G. J. Sopasis, M. Orfanoudaki, P. Zarmpas, et al., Inorg. Chem. **51**, 1170 (2012). https://doi.org/10.1021/ic2024007

44. S. I. Bezzubov, A. A. Bilyalova, I. S. Zharinova, et al., Russ. J. Inorg. Chem. **62**, 1197 (2017). https://doi.org/10.1134/S0036023617090030

45. S. I. Bezzubov, A. V. Churakov, Y. A. Belousov, et al., Cryst. Growth Des. **17**, 1166 (2017). https://doi.org/10.1021/acs.cgd.6b01563

46. W. X. Du, J. J. Zhang, S. M. Hu, et al., J. Mol. Struct. **701**, 25 (2004). https://doi.org/10.1016/j.molstruc.2004.05.011

47. Q. De. Liu, S. Gao, J. R. Li, et al., Inorg. Chem. **39**, 2488 (2000). https://doi.org/10.1021/ic990860k

48. Q. De. Liu, J. R. Li, S. Gao, et al., Eur. J. Inorg. Chem. **4**, 731 (2003). https://doi.org/10.1002/ejic.200390101

49. G. J. Sopasis, A. B. Canaj, A. Philippidis, et al., Inorg. Chem. **51**, 5911 (2012). https://doi.org/10.1021/ic300538q

50. S. Igarashi, Y. Hoshino, Y. Masuda, et al., Inorg. Chem. **39**, 2509 (2000). https://doi.org/10.1021/ic991027q

51. J. J. Zhang, S. M. Hu, S. C. Xiang, et al., J. Mol. Struct. **748**, 129 (2005). https://doi.org/10.1016/j.molstruc.2005.03.021

52. T. Komiyama, S. Igarashi, Y. Hoshino, et al., Chem. Lett. **34**, 300 (2005). https://doi.org/10.1246/cl.2005.300

53. A. Khatib and F. Aqra, Bull. Korean Chem. Soc. **30**, 2017 (2009). https://doi.org/10.5012/bkcs.2009.30.9.2017

Translated by G. Kirakosyan